HHS Public Access

Author manuscript

Cell Rep. Author manuscript; available in PMC 2021 February 25.

Published in final edited form as:

Cell Rep. 2021 February 02; 34(5): 108698. doi:10.1016/j.celrep.2021.108698.

LKB1 and AMPK instruct cone nuclear position to modify visual function

Courtney A. Burger[1,2], **Nicholas E. Albrecht**[1,2], **Danye Jiang**[1,2], **Justine H. Liang**[1,2], **Ross A. Poché**[3], **Melanie A. Samuel**[1,2,4,*]

[1]Department of Neuroscience, Baylor College of Medicine, Houston, TX 77030, USA

[2]Huffington Center on Aging, Baylor College of Medicine, Houston, TX 77030, USA

[3]Department of Molecular Physiology and Biophysics, Baylor College of Medicine, Houston, TX 77030, USA

[4]Lead contact

SUMMARY

Cone photoreceptors detect light and are responsible for color vision. These cells display a distinct polarized morphology where nuclei are precisely aligned in the apical retina. However, little is known about the mechanisms involved in cone nuclear positioning or the impact of this organization on retina function. We show that the serine/threonine kinase LKB1 and one of its substrates, AMPK, regulate cone nuclear positioning. In the absence of either molecule, cone nuclei are misplaced along the axon, resulting in altered nuclear lamination. LKB1 is required specifically in cones to mediate this process, and disruptions in nuclear alignment result in reduced cone function. Together, these results identify molecular determinants of cone nuclear position and indicate that cone nuclear position alignment enables proper visual function.

In Brief

Neuronal nuclear position is critical for circuit organization and function. Burger et al. identify LKB1 and AMPK as regulators of nuclear position in cone photoreceptors. Loss of either molecule results in mislocalized cone nuclei and altered retina function. Proper cone nuclear position may thus contribute to visual responses.

Graphical Abstract

*Correspondence: msamuel@bcm.edu.

AUTHOR CONTRIBUTIONS

C.A.B., R.A.P., and M.A.S. designed the experiments. C.A.B. conducted the primary mutant analyses, and C.A.B. and N.E.A. acquired the images. C.A.B. and D.J. conducted the histological data analyses and performed the qRT-PCR. J.H.L. reconstructed cells. C.A.B. performed electroretinography. N.E.A. performed expansion microscopy, and D.J. reconstructed cone terminals. C.A.B. generated the figures. C.A.B and M.A.S. wrote the manuscript.

DECLARATION OF INTERESTS

The authors declare no competing financial interests.

SUPPLEMENTAL INFORMATION

Supplemental Information can be found online at https://doi.org/10.1016/j.celrep.2021.108698.

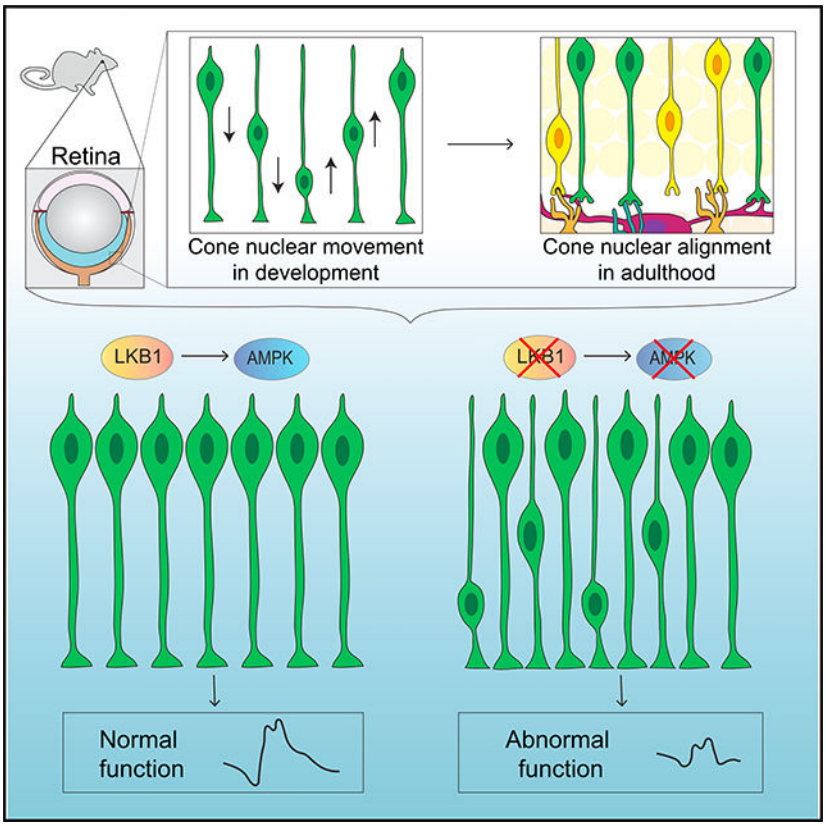

INTRODUCTION

Cell bodies in the central nervous system (CNS) are highly patterned, and this organization underlies circuit function. One such pattern is lamination where nuclei reside in neuron subtype-specific laminar positions. Although nuclear lamination is a common arrangement throughout the CNS (Nagayama et al., 2014), the mechanisms involved in nuclear positioning and the functional relevance of these patterns are relatively unknown. Nuclear laminar positioning is particularly well mapped in the retina. This highly laminated region of the CNS contains three nuclear layers, the outer nuclear layer (ONL), inner nuclear layer (INL), and ganglion cell layer (GCL), which are bounded by two synaptic layers, the inner plexiform layer (IPL) and outer plexiform layer (OPL). Specific neuron types form sublaminae within each layer that enable the retina to detect and process visual information. In particular, rod and cone photoreceptors reside in the ONL, and the nuclei of these neurons display distinct laminar patterns. Cones are responsible for daylight vision, and the diverse wavelength sensitivities of their opsins underlie color detection (Wang and Kefalov, 2011). Cone nuclei are highly polarized in diverse species ranging from humans to mice, and their cell bodies reside near the apical retina surface and are precisely aligned with one another (Carter-Dawson and LaVail, 1979; Chiquet et al., 2002; Raymond et al., 1993; Pow and Sullivan, 2007) (Figure 1A, top panel). This is in contrast to rods, which display a wide variety of nuclear positions that can vary up to 50 μm between cells, with some nuclei residing apically while others reside basally (Mattar et al., 2018; Yu et al., 2011). The

molecular mechanisms involved in generating these distinct nuclear patterns are not well understood. However, a specialized form of cone-specific nuclear movement contributes. This process is called nuclear translocation and occurs in post-mitotic cones from postnatal day (P)4 to P12 (Rich et al., 1997; Trifunović et al., 2010). During nuclear translocation, cone nuclei move throughout the ~65 μm length of the ONL in basal and apical directions along the cone axon. By P12, nuclear translocation stops as cones align their cell bodies at the apical surface of the retina, yielding cones with a stereotypical polarized nuclear position (Rich et al., 1997). However, key questions remain: why do cone nuclei need to be aligned at the retina surface, and how is nuclear translocation molecularly instructed?

To answer these questions, we focused on the serine/threonine kinase LKB1 (Liver Kinase B1, also called STK11 or Par4). LKB1 regulates 14 AMPK family kinases, AMPKα1/α2, SAD-A/-B, NUAK1/2, SIK1–3, MARK1–4, and SNRK (Lizcano et al., 2004; Jaleel et al., 2005). LKB1 was a good candidate for our studies because it plays cell-specific roles in the polarization of several neuron types, and we recently showed that this property extends to the outer retina, where it coordinates neurite remodeling to drive synapse layer emergence (Kuwako and Okano, 2018; Shelly et al., 2007; Barnes et al., 2007; Courchet et al., 2013; Burger et al., 2020). The LKB1 pathway has also been implicated in centrosome positioning, a key step in neuron migration (Asada et al., 2007; Asada and Sanada, 2010). Here, we show that LKB1 and one of its downstream kinases, AMPK, are required for cone nuclear positioning. Inactivating LKB1 in retina generally, or in cones specifically, disrupted cone nuclear alignment. Similar defects were observed in mice lacking retinal AMPK. Proper cone nuclear positioning is important for visual function as disruption of this process results in altered cone responses to light stimulation. Together, these results identify the LKB1-AMPK pathway as a molecular determinant of cone nuclear translocation and suggest that apical cone nuclear placement may facilitate visual responses.

RESULTS

LKB1 regulates cone nuclear translocation

Full-body embryonic deletion of LKB1 is lethal (Ylikorkala et al., 2001). To investigate the role of LKB1 in nuclear positioning, we used a conditional LKB1 mutant line (*LKB1*$^{F/F}$; Bardeesy et al., 2002) and crossed it to the retina progenitor-specific cre driver *Chx10-cre* (Rowan and Cepko, 2004) to generate animals lacking LKB1 specifically in the retina (hereinafter referred to as *LKB1*^{RET}). We assessed the relative position and alignment of cone nuclei in young adult animals within the ONL after staining with a cone-specific antibody to arrestin (Craft et al., 1994) and DAPI to indicate the upper and lower boundaries of the ONL. To better understand nuclear positions, we divided the ONL into four equal quadrants representing the apical (quadrant one; Q1), upper middle (quadrant two; Q2), lower middle (quadrant three; Q3), and basal (quadrant four; Q4) ONL and examined the numbers and location of cone nuclei in each quadrant (Figure 1B). In control mice, cone nuclei are localized near the apical surface of the retina, with 96.1% localized within Q1 (top 25%) of the ONL (Figures 1B and 1C). Control cone nuclei are also well aligned with each other, with an average cone nuclear position of 8.45 ± 0.2 μm, representing 13.0% of the length of the control ONL. (Figures 1B–1E). In contrast, young adult *LKB1*^{RET} mice

displayed markedly altered cone nuclear positioning: 36.7% were displaced into the lower quadrants of the ONL, compared to 3.9% in controls ($p < 0.01$; Figures 1B and 1C). Among these mislocalized nuclei, 64.0% were located in Q2, and 36.0% were located in Q3 and Q4. These displaced cones were not well aligned with one another. *LKB1*^{RET} cone nuclei were located an average of 14.6 ± 1.6 μm away from the retinal surface, representing 28.6% of the length of the *LKB1*^{RET} ONL and a 123.5% (4.1-fold) displacement from the average control cone nuclei position ($p < 0.03$; Figures 1B–1E). Thus, LKB1 is required for apical cone positioning and alignment in the ONL.

Nuclear translocation in cones occurs from P4 to P12 and modifies cone nuclear position (Yu et al., 2011; Rich et al., 1997). We thus examined control and *LKB1*^{RET} cones in detail during this period (Figures 1A and S1). This process involves nuclear descent from the apical surface toward the inner retina, followed by nuclear ascent back toward the apical surface of the ONL where cone nuclei terminate movement in their final position (Figure 1A). Our data support this model. We found that, early in translocation at P5, control cone nuclei showed an average location of 18.5 ± 1.1 μm from the apical surface and tend to be clustered in Q1 of the ONL (40.4%; Figures 1F, S1A, and S1B). As nuclear translocation proceeds in control animals, a higher percentage of cone nuclei become localized to the middle of the ONL. At P8, nuclei were located an average distance of 31.4 ± 0.6 μm from the apical surface, and only 13.0% are found within Q1, while 78.8% lie within Q2 and Q3, and 8.3% reside in Q4 (Figures 1F, S1C, and S1D). Nuclei then begin their final ascent toward the apical retina and converge at P12 toward their final position, with an average distance of 11.8 ± 0.5 μm from the apical surface, and 83.8% located within Q1 (Figures 1F, S1E, and S1F). LKB1 mutant mice displayed normal nuclear localization patterns at P5, with an average distance of 13.4 ± 0.8 μm from the apical surface ($p = 0.49$; Figures 1F, S1A, and S1B). However, this pattern differed significantly from that of controls as translocation progressed. At P8, *LKB1*^{RET} cone nuclei appeared to show slowed or directionally biased migration, with 30.7% located within Q1, while 22.3% were located in Q3 and Q4, resulting in an average distance of 22.9 ± 0.9 μm ($p < 0.0001$; Figures 1F, S1C, and S1D). At P12, these defects persisted, resulting in cone nuclei that were located further away from the apical retinal surface relative to control mice, with only 46.6% located within Q1 of the ONL ($p < 0.0001$; Figures 1F, S1E, and S1F). Nuclei were also significantly less aligned at this time point, with an average distance of 20.4 ± 2.0 μm from the apical surface ($p < 0.04$; Figure 1F). Together, these data indicate that LKB1 is required for proper movement of cone nuclei during developmental translocation.

LKB1 is required in cones to regulate their nuclear position

Next, we investigated the cellular basis of cone nuclear positioning. We asked whether there was a cell-intrinsic requirement for LKB1 in cones by selectively deleting *Lkb1* from these cells using a cone-specific Cre line (Figure 2A; *HRGP-Cre*; [Le et al., 2004], hereinafter referred to as *LKB1*^{CONE}). Because this *Cre* becomes active at P8 (Le et al.,2004; Dilan et al., 2018; Razafsky et al., 2012), this line enables us to assess the role of LKB1 specifically during nuclear translocation and bypass roles for this molecule in other aspects of retina development (Burger et al., 2020). Deletion of *Lkb1* in cones alone induced nuclear translocation defects similar to that observed in whole retina deletion (Figure 2B). Only

67.9% of cones were located in Q1 of the ONL in *LKB1*^{CONE} mice, compared to 97.1% in controls, with 23.5% and 4.8% of *LKB1*^{CONE} nuclei located in Q2 and Q3, respectively ($p < 0.0001$; Figures 2B and 2C). As expected, this disrupted cone nuclear alignment. *LKB1*^{CONE} nuclei were located an average of 13.9 ± 1.2 μm away from the apical surface, representing 22.2% of the *LKB1*^{CONE} ONL, with a relative nuclear displacement of 83.9% (3-fold) relative to control cones ($p < 0.04$; Figures 2B, 2D, and S2C). Consistent with these alterations, in *LKB1*^{CONE} mice we observed decreased mRNA levels of genes that aid in connecting microtubules to the nucleus during nuclear migration (*Syne-2*, *Sun-2*, *Dync1h1*, and *Kif5b*; Yu et al., 2011; Nakazawa and Kengaku, 2020; Figure S3A). Defects in cone nuclear position did not appear to alter other aspects of cone protein distribution or morphology as opsin localization, dorsal/ventral patterning, and pedicle morphology appeared normal in *LKB1*^{CONE} mice (Figures S3B and S3C). Finally, like *LKB1*^{RET} mice, there was no change in cone number in *LKB1*^{CONE} animals in early adulthood. However, there were fewer cones present in later adulthood, and most nuclei were aligned at the apical surface, suggesting that proper cone positioning is important for long-term cone survival (Figure S4).

To further examine the specificity of these defects, we analyzed cone position in animals in which LKB1 was deleted precisely from two other outer retina neuron subtypes, rods and horizontal cells (Figure 2A). To achieve horizontal cell- and rod-specific deletion, we crossed our *LKB1* conditional line to a horizontal cell-specific *Cre* line (*Cx57-iCre*; Hirano et al., 2016) and to a rod-specific *Cre* line (*Rdps-iCre*; Li et al., 2005) to generate *LKB1*^{HC} and *LKB1*^{ROD} mice, respectively. In both lines, cone nuclear positioning was unchanged (Figures 2E–2H, S2A, S2B, S2D, and S2E). *LKB1*^{HC} cone nuclei showed no significant difference in their nuclear placement from controls, with 80.5% and 80.3% located in Q1 at P12, respectively ($p = 0.94$; Figures 2E and 2F). Similarly, *LKB1*^{ROD} cone nuclei were placed normally relative to controls at P22, with 95.4% and 94.7% located in Q1, respectively ($p = 0.66$; Figures 2G and 2H). These data suggest that cones specifically require cell-intrinsic LKB1 signaling for nuclear translocation and proper positioning.

LKB1 functions via AMPK to regulate cone nuclear positioning

How might LKB1 signaling regulate nuclear positioning? LKB1 phosphorylates its kinase targets within a key activation loop that enables catalytic activity. Among these target proteins, AMPK was a good candidate mediator of LKB1 signaling because it is a central LKB1 target in the retina (Samuel et al., 2014). Further, AMPK activation in the retina depends almost solely on LKB1 (Samuel et al., 2014; Kim et al., 2016). To test the role of LKB1-AMPK signaling in cone nuclear positioning, we generated animals in which both alpha subunits of AMPK were specifically deleted in the retina by crossing *Prkaa1*$^{F/F}$; *Prkaa2*$^{F/F}$ (Nakada et al., 2010) animals to the retina-specific *Cre* driver *Chx10-Cre* (hereinafter referred to as *AMPK*^{RET}). The deletion of AMPK induced defects in cone nuclear positioning similar to that in *LKB1*^{RET} animals: 22.1% of nuclei were displaced from the apical retina into the lower quadrants of the ONL, compared to 3% in littermate controls ($p < 0.0001$; Figures 3A–3C). Among these displaced *AMPK*^{RET} cone nuclei, most (94%) were located in Q2. This resulted in an average cone nuclear location of 12.2 ± 0.8 μm away from the apical retinal surface, representing 19.6% of the length of the *AMPK*^{RET}

ONL, with an average displacement of 84.2% (3-fold) from the control cone nuclear position ($p \leq 0.03$; Figures 3A and 3D). Furthermore, there was no change in cone cell numbers in early adulthood (Figure S4C). These data suggest that LKB1-AMPK signaling modulates cone nuclear position. However, this does not rule out additional roles of other LKB1-dependent kinases, as the percentage of displaced cones was higher in $LKB1^{RET}$ mice (36.7%) than in $AMPK^{RET}$ mice (22.1%).

Abnormal cone nuclear positioning induces altered retina function

To determine the impact of cone nuclear positioning on visual function, we performed electroretinography (ERG) on $LKB1^{CONE}$ mice. The ERG a-wave reports on activity in photoreceptors, whereas the b-wave reports on summed synaptic responses arising from both inner and outer retina. To measure cone-driven responses, we light-adapted mice and performed ERG under photopic conditions. Light-adapted a- and b-wave amplitudes were significantly lower in $LKB1^{\mathrm{CONE}}$ animals than in controls (34% and 26% reduction, respectively; $p \leq 0.004$), indicating a defect in cone-mediated signaling (Figures 4A–4C). By contrast, rod-driven dark-adapted a- and b-wave amplitudes were unaltered in $LKB1^{CONE}$ animals relative to controls ($p \geq 0.3$; Figures 4D–4F). Given these cone-specific functional abnormalities, we questioned whether cone nuclear mispositioning may lead to disrupted connectivity with downstream synaptic partners. To examine this, we stained $LKB1^{CONE}$ retinas using antibodies specific for neuron types that form synapses with cones, bipolar cells, and horizontal cells (Table S1; Mercer and Thoreson, 2011; Tsukamoto et al., 2001; Asteriti et al., 2014). Bipolar and horizontal cell numbers were unchanged in $LKB1^{CONE}$ mice, and the morphologies of cone and rod bipolar cells were normal (Figures S5A–S5D). However, horizontal cell neurites remodeled, extending a significantly higher number of long processes into the outer retina of $LKB1^{CONE}$ mutants ($p = 0.0179$; Figures S5E and S5F). This resulted in a doubling of horizontal cell sprouts and a 42.6% increase in sprout length relative to controls ($p < 0.04$; Figure S5G). Since horizontal cell neurite remodeling is a common feature of photoreceptor dysfunction (Fariss et al., 2000; Marc et al., 2003; Samuel et al., 2014), these changes are consistent with the altered cone function we observed. Together, these data suggest that LKB1-regulated cone nuclear alignment is important for cone-driven visual responses and connectivity.

DISCUSSION

Our results suggest that LKB1 and one of its targets, AMPK, are involved in cone nuclear positioning and alignment. We found that deletion of LKB1 led to altered cone nuclear placement that results from defects in cone translocation during the second postnatal week. Using genetic methods, we found that LKB1 acts specifically in cone photoreceptors via AMPK to regulate this process. Cone nuclear mispositioning was associated with cone-specific visual defects and horizontal cell neurite remodeling. These results provide insights into the molecular pathways and functional requirement for precise cone nuclear alignment in the retina.

LKB1 as a regulator of nuclear positioning

LKB1 is a serine/threonine kinase with an increasingly recognized role as a central regulator of the nervous system (Kuwako and Okano, 2018, Shelly et al., 2007; Courchet et al., 2013; Samuel et al., 2014; Barnes et al., 2007; Asada et al., 2007; Men et al., 2015). Several recent studies suggest that, due to its broad expression and large regulatory network, the function and downstream signaling of LKB1 can vary in different neuron types and developmental stages. For example, embryonic deletion of LKB1 in hippocampal and cortical neurons delays axon formation (Barnes et al., 2007; Shelly et al., 2007; Courchet et al., 2013), but it is dispensable in the brainstem and spinal cord, which rely on SAD kinases (Lilley et al., 2013). Our results suggest an additional function for LKB1, nuclear translocation and positioning. Further, our developmental time course indicates that this defect may arise due to altered translocation kinetics. A higher percentage of LKB1-deficient cones remained in the outer ONL as control nuclei migrated inward. A few days later, more LKB1-deficient cones resided in the inner ONL, while control cones had returned to the apical retina where they remain throughout adulthood. This pattern suggests that LKB1-deficient cone nuclei can migrate, but they do so at a disrupted or perhaps slower kinetic pace than controls.

A LKB1-dependent cone nuclear movement model is supported by other molecular pathways known to impinge upon nuclear placement. These molecules include the SUN and KASH proteins, which serve to connect the inner nuclear membrane to the outer nuclear membrane and the cell cytoskeleton (Razafsky and Hodzic, 2009; Starr and Fridolfsson, 2010; Tzur et al., 2006; Hodzic et al., 2004; Haque et al., 2006). Together, this molecular structure is known as the Linker of Nucleoskeleton and Cytoskeleton (LINC) complex. Deletion of LINC family proteins disrupts nuclear positioning in *C. elegans*, *Drosophila*, and mice (Burke and Roux, 2009; Patterson et al., 2004; Tsujikawa et al., 2007). In particular, nuclear positioning defects have been observed in skeletal muscles of *Nesprin1* knockout mice, as well as in cones of *Sun1* and *Nesprin2* knockout mice (Yu et al., 2011; Zhang et al., 2007). Finally, mice lacking both *Sun1* and *Nesprin2* display cortical lamination defects and major developmental abnormalities in the CNS (Zhang et al., 2009). We find expression of these genes, along with the microtubule motor proteins dynein and kinesin, to be significantly reduced in our mutant animals, suggesting that LKB1 may directly or indirectly regulate these processes. Notably, to our knowledge, LKB1 is the only non-LINC family member to date that has been implicated in cone photoreceptor nuclear translocation.

LKB1-AMPK signaling in nuclear translocation

How might LKB1 alter nuclear placement? Although additional studies are needed to fully resolve this question, our data provide some insights. First, we show that deletion of the LKB1 target AMPK causes nuclear translocation defects similar to that observed in LKB1 mutant mice. This is notable, because we have shown that AMPK is dispensable for other early features of OPL organization (Burger et al., 2020). AMPK could participate in nuclear translocation through at least two mechanisms. It is a key regulator of energy homeostasis and maintaining AMP/ATP ratios. Since intracellular movement is energetically demanding (Wong-Riley, 2010), LKB1-AMPK-mediated energy imbalances could contribute to the phenotypes we observe. Furthermore, LKB1 and AMPK have been implicated in sensing and responding to force and directly regulating cellular scaffolds (Bays et al., 2017).

Although our data do not distinguish between these possibilities, AMPK has previously been implicated in both cell migration and microtubule dynamics, which are involved in nuclear translocation (Nakano et al., 2010; Kim et al., 2011). Second, it is possible that centrosome positioning may be involved, as this key process in migration is regulated by both LKB1 and the SUN/KASH proteins (Zhang et al., 2009; Asada and Sanada, 2010; Asada et al., 2007). Finally, we note that the nuclear translocation defects observed in AMPK-deficient animals were somewhat less severe than those in LKB1 mutant mice. Thus, additional LKB1-signaling pathways may be at least partially redundant to AMPK. Such candidates include the MARK or SAD family of kinases, which are targeted by LKB1 and are involved in microtubule organization and neuron polarization (Drewes et al., 1997; Mandelkow et al., 2004; Kishi et al., 2005; Tassan and Le Goff, 2004; Barnes et al., 2007).

Nuclear positioning and neuron function

The process that we describe here in retina may have implications in the brain. Laminar-specific positioning occurs broadly throughout the CNS, and disruptions in nuclear lamination are associated with functional decline. In particular, mutations in regulators of somal translocation (a related but distinct process) lead to neurodevelopmental defects in humans, including lissencephaly, schizophrenia, autism spectrum disorder, and epilepsy (Moon and Wynshaw-Boris, 2013; Kato and Dobyns, 2003; Guerrini and Parrini, 2010; Reiner et al., 2016; Pan et al., 2019; Bozzi et al., 2012; Muraki and Tanigaki, 2015; Ross et al., 2006). In these cases, mutations cause marked neural rearrangements and mistargeting of cells to incorrect brain regions. However, whether correct positioning of nuclei can affect neuron function is less clear. This was a particular mystery for cones, since rods, which bear many structural and functional similarities to cones, display varied nuclear arrangements. The cone-specific nuclear positioning defects we observed allowed us to assess whether cone nuclear position mattered to their function. We found marked defects specifically in cone-driven, but not rod-driven, functional responses and corresponding changes to horizontal cell neurite organization. It is interesting to speculate that such functional defects may be due to altered protein transport kinetics to cone outer segments (Yildiz and Khanna, 2012; Molday and Moritz, 2015; Lopes et al., 2010) or to altered propagation of electrical signals through cone axons (Ueno et al., 2018). Newer high-resolution microscopy or electrophysiology techniques could be brought to bear on this question. Such approaches may help resolve how the signaling pathway we uncovered in this study alters nuclear positing specifically within cones and how this, in turn, regulates light sensing or information flow.

STAR★METHODS

KEY RESOURCES TABLE

REAGENT or RESOURCE	SOURCE	IDENTIFIER
Antibodies		
Rabbit polyclonal anti-Arrestin	Millipore	Cat# Ab15282; RRIS:AB_11210270

REAGENT or RESOURCE	SOURCE	IDENTIFIER
Rabbit polyclonal anti-Calbindin	Swant	Cat# CB38; RRID:AB_10000340
Sheep polyclonal anti-Chx10	Exalpha	Cat# X1180P; RRID:AB_2314191
Goat polyclonal anti-OPN1SW	Santa Cruz	Cat# sc-14363; RRID:AB_2158332
Mouse monoclonal anti-PKC alpha	Abcam	Cat# ab31; RRID:AB_303507
Rabbit polyclonal anti-R/G Opsin	Millipore	Cat# Ab5405; RRID:AB_177456
Rabbit polyclonal anti-Secretagogin	BioVendor	Cat# RD181120100; RRID:AB_2034060
Chemicals, peptides, and recombinant proteins		
Phenylephrine HCl 2.5% Opthalmic Drops	A-S Medication Solutions LLC	N/A
Tropicamide 1% Opthalmic Drops	Akorn	Cat# 17478010212
GONAK 2.5% Hypromellose Ophthalmic Demulcent Solution	Akorn	N/A
Acryloyl-X, SE	Thermofisher	Cat# A20770
TEMED	Thermofisher	Cat# 17919
APS	Sigma Aldrich	Cat# 248614
4-Hydroxy-TEMPO	Sigma Aldrich	Cat# 176141
Sodium Acrylate	Sigma Aldrich	Cat# 408220
Acrylamide	Sigma Aldrich	Cat# A9099
N-N'-Methylenebisacrylamide	Sigma Aldrich	Cat# M7279
Sodium Chloride	Sigma Aldrich	Cat# S9888
Critical commercial assays		
RNeasy Plus Mini Kit	QIAGEN	Cat# 74104
iScript Reverse Transcription Supermix for RT-qPCR	Bio-Rad	Cat# 1708840
iTaq Universal SYBR Green Supermix	Bio-Rad	Cat# 1725120
Experimental models: organisms/strains		
Mouse: *LKB1*$^{F/F}$	Bardeesy et al., 2002	N/A
Mouse: *AMPKα1* $^{F/F}$ *α2* $^{F/F}$	Nakada et al., 2010	N/A
Mouse: *Chx10-Cre*: Tg(Chx10-EGFP/cre,-ALPP)2Clc/J	The Jackson Laboratory	RRID:MGI:3052551
Mouse: *HRGP-Cre*	Le et al., 2004	N/A
Mouse: *Rdps-iCre*	Li et al., 2005	RRID:IMSR_JAX:015850
Mouse: *Cx57-iCre*	Hirano et al., 2016	N/A
Software and algorithms		
ImageJ	NIH	https://imagej.nih.gov/ij/; RRID:SCR_003070
Imaris	Oxford Instruments	RRID:SCR_007370
PrimerBank	Spandidos et al., 2010	https://pga.mgh.harvard.edu/primerbank/; RRID:SCR_006898

REAGENT or RESOURCE	SOURCE	IDENTIFIER
$\Delta\Delta C_t$ method	Livak and Schmittgen, 2001	N/A
Prism8	Graphpad	https://www.graphpad.com; RRID:SCR_002798

RESOURCE AVAILABILITY

Lead contact—Further information and requests for resources and reagents should be directed to the Lead Contact, Melanie Samuel (msamuel@bcm.edu).

Materials availability—This study did not generate new reagents.

Data and code availability—This study did not generate datasets or codes.

EXPERIMENTAL MODEL AND SUBJECT DETAILS

The *LKB1* conditional null mutant (*LKB1*$^{F/F}$) has been described previously (Bardeesy et al., 2002, provided by R. DePinho, MD Anderson Cancer Center). To delete *Lkb1* in the retina, *LKB1*$^{F/F}$ mice were crossed to *Chx10-Cre* animals (Rowan and Cepko, 2004, provided by Constance Cepko, Harvard University) to generate animals referred to here as *LKB1*^{RET} mice. To delete LKB1 in cones, we crossed *LKB1*$^{F/F}$ animals to the *HRGP-Cre* line (Le et al., 2004, provided by Yun-Zheng Le, University of Oklahoma) to generate animals referred to as *LKB1*^{CONE} mice. To delete LKB1 either in horizontal cells or rods, we crossed *LKB1*$^{F/F}$ animals to the *Cx57-iCre* line (Hirano et al., 2016, provided by Nicholas Brecha, UCLA) or to the *Rdps-iCre* line (Li et al., 2005) to generate animals referred to as *LKB1*^{HC} mice and *LKB1*^{ROD} mice, respectively. For all of these lines, *LKB1*$^{F/F}$ littermates were used as controls. The *AMPK* conditional null mutant *Prkaa1*$^{F/F}$*Prkaa2*$^{F/F}$ has been previously described (Nakada et al., 2010, provided by Dr. Daisuke Nakada, Baylor College of Medicine). To broadly delete both alpha subunits of *Ampk* (*Prkaa1 and Prkaa2*) in the retina, *Prkaa1*$^{F/F}$*Prkaa2*$^{F/F}$ mice were crossed to *Chx10-Cre* to generate animals referred to as *AMPK*^{RET} mice. For this line, *Prkaa1*$^{F/F}$*Prkaa2*$^{F/F}$ littermates were used as controls. Eyes were collected from animals at P5, P8, P12, P22, 7 months, and 1 year. Experiments were carried out in male and female mice in accordance with the recommendations in the Guide for the Care and Use of Laboratory Animals of the NIH under protocols approved by the BCM Institutional Animal Care and Use Committee.

METHOD DETAILS

Immunohistochemistry—For dorsal ventral patterning, a hole was made in the right cornea in the nasal position, with dorsal being up and ventral being down. Whole eyes were fixed for 45 min in 4% paraformaldehyde and then rinsed with PBS. Cryosections of retinas were prepared as previously described (Samuel et al., 2014). Eyecups were dissected by removing the cornea and lens. Retinas were then cryoprotected in 30% sucrose, embedded in Optimal Cutting Temperature (OCT) compound, placed in methyl butane on dry ice for freezing, and then sectioned at 20 μm, followed by mounting on Superfrost Plus slides. Slides were incubated with blocking solution (3% normal donkey serum and 0.3% Triton

X-100 in PBS) for 1 hour at room temperature and then incubated with primary antibodies (Table S1) overnight at 4°C. Slides were washed with PBS three times for 10 min and incubated with secondary antibodies (1:1000 dilution) for 1 hour at room temperature. Slides were again washed three times with PBS for 10 min. Samples were mounted in Vectashield. Images were acquired on an Olympus Fluoview FV1200 confocal microscope and processed using Fiji. 3D rendered cones were generated using Imaris.

Electroretinography—We performed ERG on adult one-month-old mice as previously described (Albrecht et al., 2018). In brief, mice were dark-adapted overnight and anesthetized with 1.5% isoflurane at an oxygen flow rate of 1.0 L/min. Mice were placed on a heated platform and pupils were dilated using phenylephrine hydrochloride and tropicamide. Gonak solution was placed on the cornea, and a contact lens-style electrode was placed on top to monitor electroretinograms from each eye. For scotopic responses, a ground electrode was placed subcutaneously into the forehead, while a reference electrode was placed in the haunch. The Diagnosys Celeris ERG system was used to elicit both scotopic and photopic responses. Scotopic responses were elicited in the dark with flashes ranging from 0.003 cd*s/m^2 to 20.0 cd*s/m^2. Photopic responses were elicited after eyes had been adapted to light for five minutes at a flash of 10.0 cd*s/m^2.

Whole retina qRT-PCR—Retinas from P22 control and $LKB1^{CONE}$ mice were dissected in ice-cold RNase-free water, and each pair of retinas were homogenized separately. Total RNA was purified from each sample using a RNeasy Plus Mini Kit according to the manufacturer's instruction (QIAGEN). First strand cDNA synthesis was performed using a complementary DNA synthesis kit according to the manufacturer's protocol (iScript Reverse Transcription Supermix for qRT-PCR; Bio-Rad Laboratories Inc.). Quantitative real-time PCR (qRT-PCR) was performed with forward and reverse primers (Table S2) to targets and house-keeping genes using iTaq Universal SYBR Green Supermix (Bio-Rad) and a CFX384 Touch Real-Time PCR Detection System (Bio-Rad). Relative quantification was determined using the $\Delta\Delta C_t$ method (Livak and Schmittgen, 2001). Genes of interest were normalized to 18S rRNA (Adachi et al., 2015). Primers were designed using the PrimerBank software (Spandidos et al., 2010).

Expansion microscopy—Expansion microscopy was performed as previously described (Asano et al., 2018; Burger et al., 2020). In brief, tissue samples were prepared for immunohistochemistry as described above. After the final PBS wash, samples were immersed in a 0.1mg/mL solution of Acryloyl-X (AcX) for 4 hours at room temperature. Following this, samples were washed 3 times in 1X PBS for 10 min prior to gelation. To form the hydrophilic gel around the samples a 47:1:1:1 solution of Stock X: TEMED (0.1mg/mL): APS (0.1mg/mL): 4-hydroxy-TEMPO (5.0mg/mL) were placed within chambers surrounding the tissue slices. Stock X solution was made using 38 g of sodium acrylate, 50 g of acrylamide, 2 g of N,N'-Methylenebisacrylamide, and 29.2 g of sodium chloride in a total volume of 100 mL using 10X PBS stock. Slides were incubated at 4°C for 1 hour followed by incubation at 37°C for an additional three hours to allow gel to fully set. Once solidified, excess gel was removed and slides were placed into deionized water for one hour, replacing water every 15 minutes. Individual gels with tissue sample were mounted in

deep chambers with fresh deionized water surrounding the sample and imaged on an Olympus Fluoview FV1200 confocal microscope and processed using Imaris.

QUANTIFICATION AND STATISTICAL ANALYSIS

Histological quantification—All quantification was performed using retinal sections prepared from *LKB1*^{RET}, *LKB1*^{CONE}, *LKB1*^{ROD}, *LKB1*^{HC}, AMPK^{RET} and control animals at ages from P5 to P30. Littermate controls were used in all experiments, and all images were acquired at equivalent retinal eccentricities from the optic nerve head. For all experiments, data were collected from two to five mice per group, and three to four images per animal were obtained. To quantify distance of nuclei from the apical surface, antibodies to OPN1SW or MCAR were used to label cones, and DAPI was used to label nuclei and demarcate the boundaries of the ONL. The distance of cone nuclei from the apical surface was measured, and values were normalized to the length of the ONL. Normalized values were then averaged. Nuclei were binned into the first, second, third, or fourth quadrant based on whether they fell within the 0%–25%, 25%–50%, 50%–75%, or 75%–100% regions of the ONL, respectively. To determine the displacement of individual nuclei, the absolute value of the difference between the normalized average of all control nuclei from the apical surface from the normalized distance of an individual nuclei were calculated and divided by the normalized average of all control nuclei. To quantify the number of cones, rod bipolar cells, and cone bipolar cells, antibodies against MCAR, PKCα, and Secretagogin were used, respectively. The number of cells within an image (211.97 × 211.97 μm^2) were counted and values were averaged. For ectopically localized horizontal cell neurites, horizontal cells were labeled with an antibody against calbindin and DAPI was used to visualize the nuclei. To quantify ectopic neurites, HC sprouts that extended one or more nuclei above the OPL were counted and their lengths measured.

Statistical analysis—Analyses of ERG results and percent of cone nuclei in a quadrant were performed using an unpaired t test across rows with quantifications corrected for multiple comparisons using the Holm-Sidak method. Analyses of the average distance of nuclei from the apical surface, displacement of nuclei from the control average apical distance, number of cones, number of bipolar cells, number of horizontal sprouts, and length of horizontal sprouts were performed using a non-parametric Mann-Whitney Rank Sum U-test. Analysis of qRT-PCR was done using an unpaired two-tailed Student's t test. Statistical differences were evaluated using GraphPad Prism 8 software. $p < 0.05$ was considered statistically significant.

Supplementary Material

Refer to Web version on PubMed Central for supplementary material.

ACKNOWLEDGMENTS

We thank Elizabeth Zuniga-Sanchez and members of our laboratory for scientific discussions and advice. We thank Hui Zheng's laboratory for the use of Imaris, Daisuke Nakada for providing the AMPK mice, and Nicholas Brecha for providing the Cx57-iCre mice. This work was supported by the National Institutes of Health (NIH; DP2EY02798, 1R56AG061808, and R01EY030458 to M.A.S.), the Cancer Prevention Research Institute of Texas, and the Brain Research Foundation. C.A.B. was supported by the NIH and the National Eye Institute under award

number T32EY007001. N.E.A. was supported by the NIH and the National Institute of General Medical Sciences under award number T32GM088129.

REFERENCES

Adachi H, Tominaga H, Maruyama Y, Yoneda K, Maruyama K, Yoshii K, Kinoshita S, Nakano M, and Tashiro K (2015). Stage-specific reference genes significant for quantitative PCR during mouse retinal development. Genes Cells 20, 625–635. [PubMed: 26059597]

Albrecht NE, Alevy J, Jiang D, Burger CA, Liu BI, Li F, Wang J, Kim SY, Hsu CW, Kalaga S, et al. (2018). Rapid and integrative discovery of retina regulatory molecules. Cell Rep. 24, 2506–2519. [PubMed: 30157441]

Asada N, and Sanada K (2010). LKB1-mediated spatial control of GSK3beta and adenomatous polyposis coli contributes to centrosomal forward movement and neuronal migration in the developing neocortex. J. Neurosci. 30, 8852–8865. [PubMed: 20592207]

Asada N, Sanada K, and Fukada Y (2007). LKB1 regulates neuronal migration and neuronal differentiation in the developing neocortex through centrosomal positioning. J. Neurosci. 27, 11769–11775. [PubMed: 17959818]

Asano SM, Gao R, Wassie AT, Tillberg PW, Chen F, and Boyden ES (2018). Expansion microscopy: protocols for imaging proteins and RNA in cells and tissue. Curr. Protoc. Cell Biol. 80, e56. [PubMed: 30070431]

Asteriti S, Gargini C, and Cangiano L (2014). Mouse rods signal through gap junctions with cones. eLife 3, e01386. [PubMed: 24399457]

Bardeesy N, Sinha M, Hezel AF, Signoretti S, Hathaway NA, Sharpless NE, Loda M, Carrasco DR, and DePinho RA (2002). Loss of the Lkb1 tumour suppressor provokes intestinal polyposis but resistance to transformation. Nature 419, 162–167. [PubMed: 12226664]

Barnes AP, Lilley BN, Pan YA, Plummer LJ, Powell AW, Raines AN, Sanes JR, and Polleux F (2007). LKB1 and SAD kinases define a pathway required for the polarization of cortical neurons. Cell 129, 549–563. [PubMed: 17482548]

Bays JL, Campbell HK, Heidema C, Sebbagh M, and DeMali KA (2017). Linking E-cadherin mechanotransduction to cell metabolism through force-mediated activation of AMPK. Nat. Cell Biol. 19, 724–731. [PubMed: 28553939]

Bozzi Y, Casarosa S, and Caleo M (2012). Epilepsy as a neurodevelopmental disorder. Front. Psychiatry 3, 19. [PubMed: 22457654]

Burger CA, Alevy J, Casasent AK, Jiang D, Albrecht NE, Liang JH, Hirano AA, Brecha NC, and Samuel MA (2020). LKB1 coordinates neurite remodeling to drive synapse layer emergence in the outer retina. eLife 9, e56931. [PubMed: 32378514]

Burke B, and Roux KJ (2009). Nuclei take a position: managing nuclear location. Dev. Cell 17, 587–597. [PubMed: 19922864]

Carter-Dawson LD, and LaVail MM (1979). Rods and cones in the mouse retina. I. Structural analysis using light and electron microscopy. J. Comp. Neurol. 188, 245–262. [PubMed: 500858]

Chiquet C, Dkhissi-Benyahya O, Chounlamountri N, Szel A, Degrip WJ, and Cooper HM (2002). Characterization of calbindin-positive cones in primates. Neuroscience 115, 1323–1333. [PubMed: 12453500]

Courchet J, Lewis TL Jr., Lee S, Courchet V, Liou DY, Aizawa S, and Polleux F (2013). Terminal axon branching is regulated by the LKB1-NUAK1 kinase pathway via presynaptic mitochondrial capture. Cell 153, 1510–1525. [PubMed: 23791179]

Craft CM, Whitmore DH, and Wiechmann AF (1994). Cone arrestin identified by targeting expression of a functional family. J. Biol. Chem. 269, 4613–4619. [PubMed: 8308033]

Dilan TL, Singh RK, Saravanan T, Moye A, Goldberg AFX, Stoilov P, and Ramamurthy V (2018). Bardet-Biedl syndrome-8 (BBS8) protein is crucial for the development of outer segments in photoreceptor neurons. Hum. Mol. Genet. 27, 283–294. [PubMed: 29126234]

Drewes G, Ebneth A, Preuss U, Mandelkow EM, and Mandelkow E (1997). MARK, a novel family of protein kinases that phosphorylate microtubule-associated proteins and trigger microtubule disruption. Cell 89, 297–308. [PubMed: 9108484]

Fariss RN, Li ZY, and Milam AH (2000). Abnormalities in rod photoreceptors, amacrine cells, and horizontal cells in human retinas with retinitis pigmentosa. Am. J. Ophthalmol. 129, 215–223. [PubMed: 10682975]

Guerrini R, and Parrini E (2010). Neuronal migration disorders. Neurobiol. Dis. 38, 154–166. [PubMed: 19245832]

Haque F, Lloyd DJ, Smallwood DT, Dent CL, Shanahan CM, Fry AM, Trembath RC, and Shackleton S (2006). SUN1 interacts with nuclear lamin A and cytoplasmic nesprins to provide a physical connection between the nuclear lamina and the cytoskeleton. Mol. Cell. Biol. 26, 3738–3751. [PubMed: 16648470]

Hirano AA, Liu X, Boulter J, Grove J, Pérez de Sevilla Müller L, Barnes S, and Brecha NC (2016). Targeted deletion of vesicular GABA transporter from retinal horizontal cells eliminates feedback modulation of photoreceptor calcium channels. eNeuro 3, ENEURO.0148–15.2016.

Hodzic DM, Yeater DB, Bengtsson L, Otto H, and Stahl PD (2004). Sun2 is a novel mammalian inner nuclear membrane protein. J. Biol. Chem. 279, 25805–25812. [PubMed: 15082709]

Jaleel M, McBride A, Lizcano JM, Deak M, Toth R, Morrice NA, and Alessi DR (2005). Identification of the sucrose non-fermenting related kinase SNRK, as a novel LKB1 substrate. FEBS Lett. 579, 1417–1423. [PubMed: 15733851]

Kato M, and Dobyns WB (2003). Lissencephaly and the molecular basis of neuronal migration. Hum. Mol. Genet. 12, R89–R96. [PubMed: 12668601]

Kim EK, Park JM, Lim S, Choi JW, Kim HS, Seok H, Seo JK, Oh K, Lee DS, Kim KT, et al. (2011). Activation of AMP-activated protein kinase is essential for lysophosphatidic acid-induced cell migration in ovarian cancer cells. J. Biol. Chem. 286, 24036–24045. [PubMed: 21602274]

Kim J, Yang G, Kim Y, Kim J, and Ha J (2016). AMPK activators: mechanisms of action and physiological activities. Exp. Mol. Med. 48, e224. [PubMed: 27034026]

Kishi M, Pan YA, Crump JG, and Sanes JR (2005). Mammalian SAD kinases are required for neuronal polarization. Science 307, 929–932. [PubMed: 15705853]

Kuwako KI, and Okano H (2018). Versatile roles of LKB1 kinases signaling in neural development and homeostasis. Front. Mol. Neurosci. 11, 354. [PubMed: 30333724]

Le YZ, Ash JD, Al-Ubaidi MR, Chen Y, Ma JX, and Anderson RE (2004). Targeted expression of Cre recombinase to cone photoreceptors in transgenic mice. Mol. Vis. 10, 1011–1018. [PubMed: 15635292]

Li S, Chen D, Sauvé Y, McCandless J, Chen YJ, and Chen CK (2005). Rhodopsin-iCre transgenic mouse line for Cre-mediated rod-specific gene targeting. Genesis 41, 73–80. [PubMed: 15682388]

Lilley BN, Pan YA, and Sanes JR (2013). SAD kinases sculpt axonal arbors of sensory neurons through long- and short-term responses to neurotrophin signals. Neuron 79, 39–53. [PubMed: 23790753]

Livak KJ, and Schmittgen TD (2001). Analysis of relative gene expression data using real-time quantitative PCR and the 2(-Delta Delta C(T)) Method. Methods 25, 402–408. [PubMed: 11846609]

Lizcano JM, Göransson O, Toth R, Deak M, Morrice NA, Boudeau J, Hawley SA, Udd L, Mäkelä TP, Hardie DG, and Alessi DR (2004). LKB1 is a master kinase that activates 13 kinases of the AMPK subfamily, including MARK/PAR-1. EMBO J. 23, 833–843. [PubMed: 14976552]

Lopes VS, Jimeno D, Khanobdee K, Song X, Chen B, Nusinowitz S, and Williams DS (2010). Dysfunction of heterotrimeric kinesin-2 in rod photoreceptor cells and the role of opsin mislocalization in rapid cell death. Mol. Biol. Cell 21, 4076–4088. [PubMed: 20926680]

Mandelkow EM, Thies E, Trinczek B, Biernat J, and Mandelkow E (2004). MARK/PAR1 kinase is a regulator of microtubule-dependent transport in axons. J. Cell Biol. 167, 99–110. [PubMed: 15466480]

Marc RE, Jones BW, Watt CB, and Strettoi E (2003). Neural remodeling in retinal degeneration. Prog. Retin. Eye Res. 22, 607–655. [PubMed: 12892644]

Mattar P, Stevanovic M, Nad I, and Cayouette M (2018). Casz1 controls higher-order nuclear organization in rod photoreceptors. PNAS 115, E7987–E7996. [PubMed: 30072429]

Men Y, Zhang A, Li H, Zhang T, Jin Y, Li H, Zhang J, and Gao J (2015). LKB1 is required for the development and maintenance of stereocilia in inner ear hair cells in mice. PLoS ONE 10, e0135841. [PubMed: 26274331]

Mercer AJ, and Thoreson WB (2011). The dynamic architecture of photoreceptor ribbon synapses: cytoskeletal, extracellular matrix, and intramembrane proteins. Vis. Neurosci. 28, 453–471. [PubMed: 22192503]

Molday RS, and Moritz OL (2015). Photoreceptors at a glance. J. Cell Sci. 128, 4039–4045. [PubMed: 26574505]

Moon HM, and Wynshaw-Boris A (2013). Cytoskeleton in action: lissencephaly, a neuronal migration disorder. Wiley Interdiscip. Rev. Dev. Biol. 2, 229–245. [PubMed: 23495356]

Muraki K, and Tanigaki K (2015). Neuronal migration abnormalities and its possible implications for schizophrenia. Front. Neurosci. 9, 74. [PubMed: 25805966]

Nagayama S, Homma R, and Imamura F (2014). Neuronal organization of olfactory bulb circuits. Front. Neural Circuits 8, 98. [PubMed: 25232305]

Nakada D, Saunders TL, and Morrison SJ (2010). Lkb1 regulates cell cycle and energy metabolism in haematopoietic stem cells. Nature 468, 653–658. [PubMed: 21124450]

Nakano A, Kato H, Watanabe T, Min KD, Yamazaki S, Asano Y, Seguchi O, Higo S, Shintani Y, Asanuma H, et al. (2010). AMPK controls the speed of microtubule polymerization and directional cell migration through CLIP-170 phosphorylation. Nat. Cell Biol. 12, 583–590. [PubMed: 20495555]

Nakazawa N, and Kengaku M (2020). Mechanical regulation of nuclear translocation in migratory neurons. Front. Cell Dev. Biol. 8, 150. [PubMed: 32226788]

Pan YH, Wu N, and Yuan XB (2019). Toward a better understanding of neuronal migration deficits in autism spectrum disorder. Front. Cell Dev. Biol. 7, 205. [PubMed: 31620440]

Patterson K, Molofsky AB, Robinson C, Acosta S, Cater C, and Fischer JA (2004). The functions of Klarsicht and nuclear lamin in developmentally regulated nuclear migrations of photoreceptor cells in the Drosophila eye. Mol. Biol. Cell 15, 600–610. [PubMed: 14617811]

Pow DV, and Sullivan RK (2007). Nuclear kinesis, neurite sprouting and abnormal axonal projections of cone photoreceptors in the aged and AMD-afflicted human retina. Exp. Eye Res. 84, 850–857. [PubMed: 17343852]

Raymond PA, Barthel LK, Rounsifer ME, Sullivan SA, and Knight JK (1993). Expression of rod and cone visual pigments in goldfish and zebrafish: a rhodopsin-like gene is expressed in cones. Neuron 10, 1161–1174. [PubMed: 8318234]

Razafsky D, and Hodzic D (2009). Bringing KASH under the SUN: the many faces of nucleo-cytoskeletal connections. J. Cell Biol. 186, 461–472. [PubMed: 19687252]

Razafsky D, Blecher N, Markov A, Stewart-Hutchinson PJ, and Hodzic D (2012). LINC complexes mediate the positioning of cone photoreceptor nuclei in mouse retina. PLoS ONE 7, e47180. [PubMed: 23071752]

Reiner O, Karzbrun E, Kshirsagar A, and Kaibuchi K (2016). Regulation of neuronal migration, an emerging topic in autism spectrum disorders. J. Neurochem. 136, 440–456. [PubMed: 26485324]

Rich KA, Zhan Y, and Blanks JC (1997). Migration and synaptogenesis of cone photoreceptors in the developing mouse retina. J. Comp. Neurol. 388, 47–63. [PubMed: 9364238]

Ross CA, Margolis RL, Reading SAJ, Pletnikov M, and Coyle JT (2006). Neurobiology of schizophrenia. Neuron 52, 139–153. [PubMed: 17015232]

Rowan S, and Cepko CL (2004). Genetic analysis of the homeodomain transcription factor Chx10 in the retina using a novel multifunctional BAC transgenic mouse reporter. Dev. Biol. 271, 388–402. [PubMed: 15223342]

Samuel MA, Voinescu PE, Lilley BN, de Cabo R, Foretz M, Viollet B, Pawlyk B, Sandberg MA, Vavvas DG, and Sanes JR (2014). LKB1 and AMPK regulate synaptic remodeling in old age. Nat. Neurosci. 17, 1190–1197. [PubMed: 25086610]

Shelly M, Cancedda L, Heilshorn S, Sumbre G, and Poo MM (2007). LKB1/STRAD promotes axon initiation during neuronal polarization. Cell 129, 565–577. [PubMed: 17482549]

Spandidos A, Wang X, Wang H, and Seed B (2010). PrimerBank: a resource of human and mouse PCR primer pairs for gene expression detection and quantification. Nucleic Acids Res. 38, D792–D799. [PubMed: 19906719]

Starr DA, and Fridolfsson HN (2010). Interactions between nuclei and the cytoskeleton are mediated by SUN-KASH nuclear-envelope bridges. Annu. Rev. Cell Dev. Biol. 26, 421–444. [PubMed: 20507227]

Tassan JP, and Le Goff X (2004). An overview of the KIN1/PAR-1/MARK kinase family. Biol. Cell 96, 193–199. [PubMed: 15182702]

Trifunović D, Dengler K, Michalakis S, Zrenner E, Wissinger B, and Paquet-Durand F (2010). cGMP-dependent cone photoreceptor degeneration in the cpfl1 mouse retina. J. Comp. Neurol. 518, 3604–3617. [PubMed: 20593360]

Tsujikawa M, Omori Y, Biyanwila J, and Malicki J (2007). Mechanism of positioning the cell nucleus in vertebrate photoreceptors. Proc. Natl. Acad. Sci. USA 104, 14819–14824. [PubMed: 17785424]

Tsukamoto Y, Morigiwa K, Ueda M, and Sterling P (2001). Microcircuits for night vision in mouse retina. J. Neurosci. 21, 8616–8623. [PubMed: 11606649]

Tzur YB, Wilson KL, and Gruenbaum Y (2006). SUN-domain proteins: 'Velcro' that links the nucleoskeleton to the cytoskeleton. Nat. Rev. Mol. Cell Biol. 7, 782–788. [PubMed: 16926857]

Ueno A, Omori Y, Sugita Y, Watanabe S, Chaya T, Kozuka T, Kon T, Yoshida S, Matsushita K, Kuwahara R, et al. (2018). Lrit1, a retinal transmembrane protein, regulates selective synapse formation in cone photoreceptor cells and visual acuity. Cell Rep. 22, 3548–3561. [PubMed: 29590622]

Wang JS, and Kefalov VJ (2011). The cone-specific visual cycle. Prog. Retin. Eye Res. 30, 115–128. [PubMed: 21111842]

Wong-Riley MT (2010). Energy metabolism of the visual system. Eye Brain 2, 99–116. [PubMed: 23226947]

Yildiz O, and Khanna H (2012). Ciliary signaling cascades in photoreceptors. Vision Res. 75, 112–116. [PubMed: 22921640]

Ylikorkala A, Rossi DJ, Korsisaari N, Luukko K, Alitalo K, Henkemeyer M, and Mäkelä TP (2001). Vascular abnormalities and deregulation of VEGF in Lkb1-deficient mice. Science 293, 1323–1326. [PubMed: 11509733]

Yu J, Lei K, Zhou M, Craft CM, Xu G, Xu T, Zhuang Y, Xu R, and Han M (2011). KASH protein Syne-2/Nesprin-2 and SUN proteins SUN1/2 mediate nuclear migration during mammalian retinal development. Hum. Mol. Genet. 20, 1061–1073. [PubMed: 21177258]

Zhang X, Xu R, Zhu B, Yang X, Ding X, Duan S, Xu T, Zhuang Y, and Han M (2007). Syne-1 and Syne-2 play crucial roles in myonuclear anchorage and motor neuron innervation. Development 134, 901–908. [PubMed: 17267447]

Zhang X, Lei K, Yuan X, Wu X, Zhuang Y, Xu T, Xu R, and Han M (2009). SUN1/2 and Syne/Nesprin-1/2 complexes connect centrosome to the nucleus during neurogenesis and neuronal migration in mice. Neuron 64, 173–187. [PubMed: 19874786]

Highlights

- Identify LKB1 as a key regulator of cone nuclear positioning
- Demonstrate that LKB1 functions specifically in cones
- Reveal AMPK as a downstream cone nuclear positioning regulator
- Establish a role for cone nuclear position in visual function

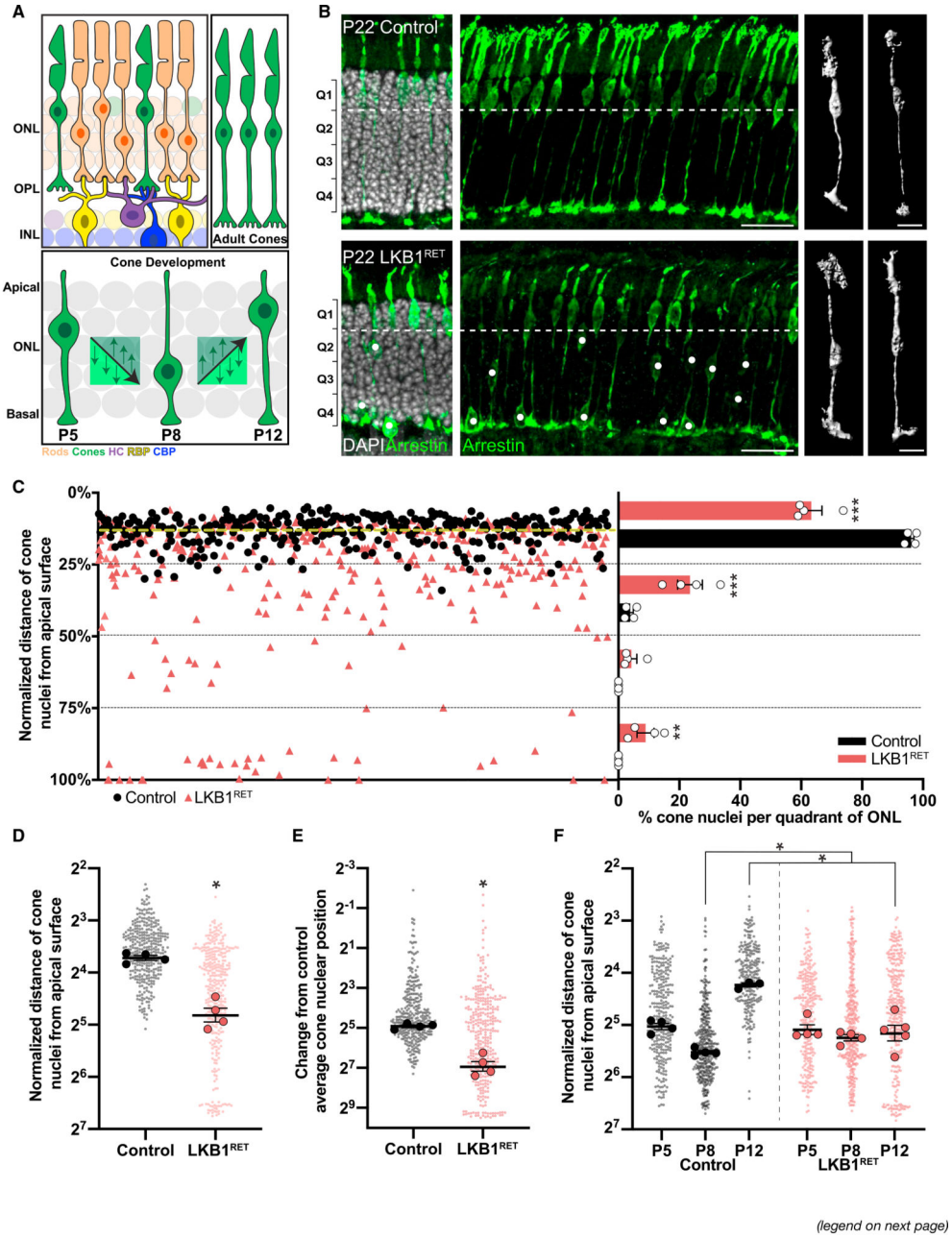

(legend on next page)

Figure 1. Cone nuclear position is altered with loss of LKB1

(A) Schematic of the relative organization of outer retina neurons in adults (top panel) and cone nuclear translocation in development (bottom panel). The outer nuclear layer (ONL) contains cones (green), whose nuclei are located at the apical surface of the ONL, and rods (orange), whose nuclei are located throughout the ONL. During development, cones are localized apically at P5 followed by net movement toward the inner retina at P8. By P12, most cone nuclei have returned to the outer retina where they align and adopt their final position at the apical retina surface. Green arrows indicate the potential for apical and basal

micromovements as translocation proceeds. Mature cones and rods form synaptic connections in the outer plexiform layer (OPL) with horizontal cells (purple), rod bipolar cells (yellow), and cone bipolar cells (blue) located in the inner nuclear layer (INL).

(B) Representative images and reconstructions of cones (anti-arrestin, green; DAPI, gray) in control and *LKB1*^{RET} mice at P22. Numerous *LKB1*^{RET} cones display nuclear position defects (white dots). Q1, Q2, Q3, and Q4 indicate quadrants one through four, respectively. The white dashed line indicates the lower boundary of ONL Q1.

(C) Scatterplot and graph displaying the location and the percent quantification of cone nuclei normalized to the length of the ONL in control (black) and *LKB1*^{RET} (red) mice in each ONL quadrant. There is a significant decrease in the number of *LKB1*^{RET} nuclei in the outer half of the ONL and an increase in *LKB1*^{RET} nuclei number in the inner half of the ONL relative to controls (n = 338 and 352 cells from 4 control and 4 *LKB1*^{RET} mice, respectively). The yellow dashed line demarks the average normalized cone nuclear position in controls.

(D and E) Quantification of the average normalized distance of cone nuclei from the apical surface of the outer retina (D) and the average nuclear displacement from control cone nuclear position (E). There is a significant increase in both the average distance and the average nuclear displacement of *LKB1*^{RET} mice relative to controls (n = 338 and 352 cells from 4 control and 4 *LKB1*^{RET} mice, respectively).

(F) Relative average positions of normalized control and *LKB1*^{RET} cone nuclei over development at P5, P8, and P12. No significant difference is observed at P5. However, by P8, *LKB1*^{RET} cones are significantly closer to the apical retina, and at P12, they are located significantly more basally relative to controls, resulting in an increase in the average nuclear distance (P5, n = 289 and 304 cells from 4 control and 4 *LKB1*^{RET} mice, respectively; P8, n = 440 and 390 cells from 4 control and 4 *LKB1*^{RET} mice, respectively; P12, n = 250 and 357 cells from 3 control and 5 *LKB1*^{RET} mice, respectively).

Scale bars, 25 μm and 5 μm for reconstructions. Data are represented as mean ± SEM (C) or as beeswarm SuperPlots (D–F) in which individual cone nuclei values are presented together with the mean from each animal ± SEM. **$p < 0.001$; ***$p < 0.01$, unpaired two-tailed Student's t test in (C). *$p < 0.05$, non-parametric Mann-Whitney rank-sum U test in (D)–(F).

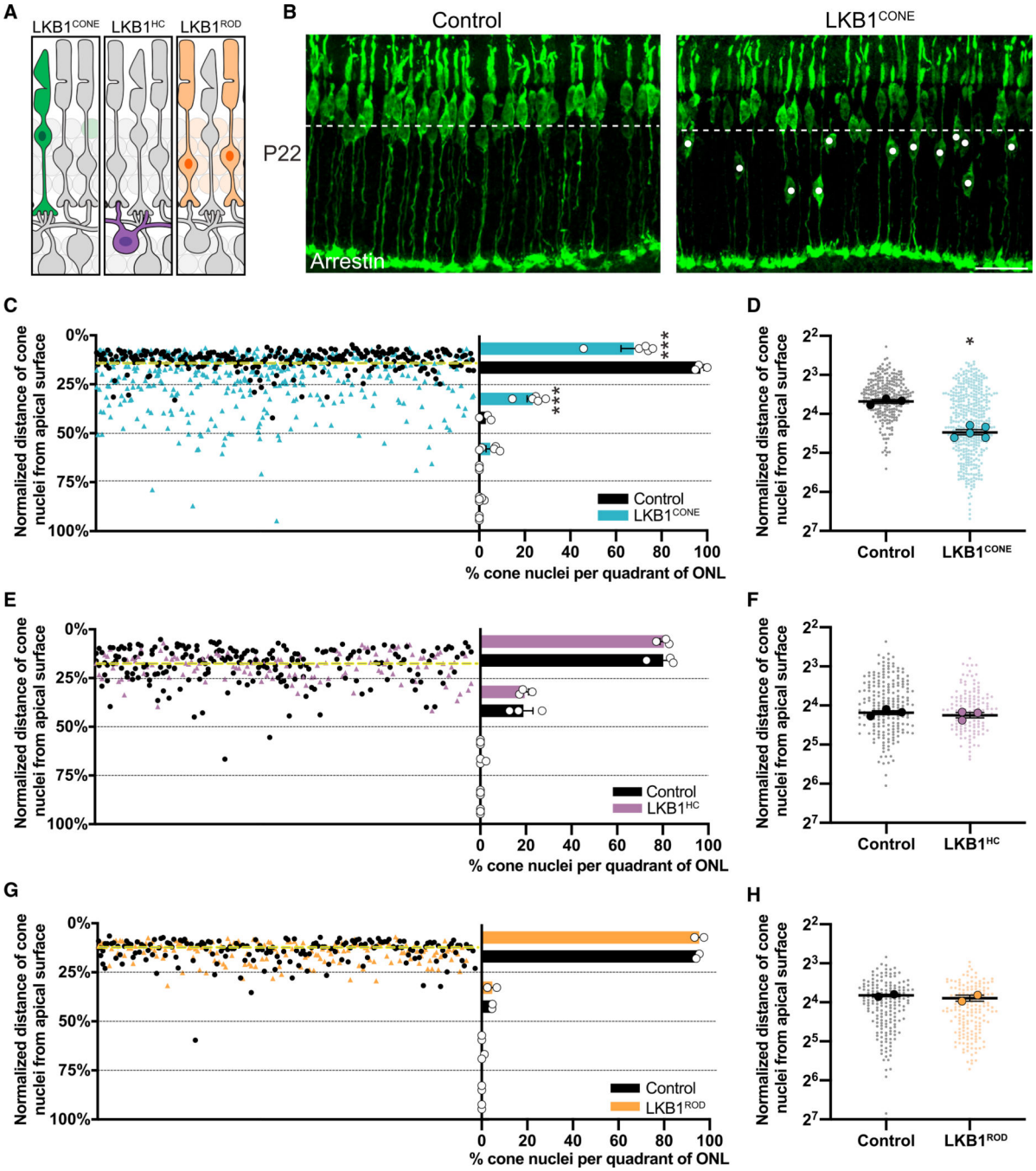

Figure 2. LKB1 is required specifically in cones for nuclear translocation

(A) Schematic of mouse models in which LKB1 is deleted in distinct neuron types using *Cre* lines that induce knockout of *Lkb1* specifically in cones (*HRGP-Cre*, green), horizontal cells (*Cx57-iCre*, purple), or rods (*Rdps-iCre*, orange).

(B) Representative images of cones (anti-arrestin, green) in control and $LKB1^{CONE}$ mice at P22. Numerous cone nuclei in $LKB1^{CONE}$ mice display position defects (white dots). The white dashed line indicates the lower boundary of ONL Q1.

(C) Scatterplot and graph displaying the location and percent quantification of cone nuclei normalized to the length of the ONL in control (black) and $LKB1^{CONE}$ mice (blue) in each ONL quadrant. There is a significant decrease in the number of $LKB1^{CONE}$ nuclei in the outer half of the ONL relative to controls (n = 266 and 415 cells from 3 control and 5 $LKB1^{CONE}$ mice, respectively).

(D) Quantification of the average normalized distance of cone nuclei from the apical retina surface. There is a significant increase in the average distance of cone nuclei in $LKB1^{CONE}$ mice relative to controls (n = 266 and 415 cells from 3 control and 5 $LKB1^{CONE}$ mice, respectively).

(E–H) Scatterplots and graphs displaying the normalized position, percent quantification, and average distance of normalized cone nuclei from the apical surface of the outer retina in $LKB1^{HC}$ mice (purple; E and F) or $LKB1^{ROD}$ mice (orange; G and H) and paired controls. There is no change in the number of cone nuclei located in each quadrant in either mutant line (E and G) or in the number of mislocalized cone nuclei (F and H; n = 204 control and 131 $LKB1^{HC}$ cells from 3 control and 3 $LKB1^{HC}$ mice, respectively; n = 173 and 169 cells from 2 control and 2 $LKB1^{ROD}$ mice, respectively).

Scale bars, 25 μm. Yellow dashed lines indicate the average normalized cone nuclear position in controls. Data are represented as mean ± SEM (C, E, and G) or as beeswarm SuperPlots (D, F, and H) in which individual cone nuclei values are presented together with the mean from each animal as the mean ± SEM. ***$p < 0.001$, unpaired two-tailed Student's t test (C, E, and G); *$p < 0.05$, non-parametric Mann-Whitney rank-sum U test (D, F, and H).

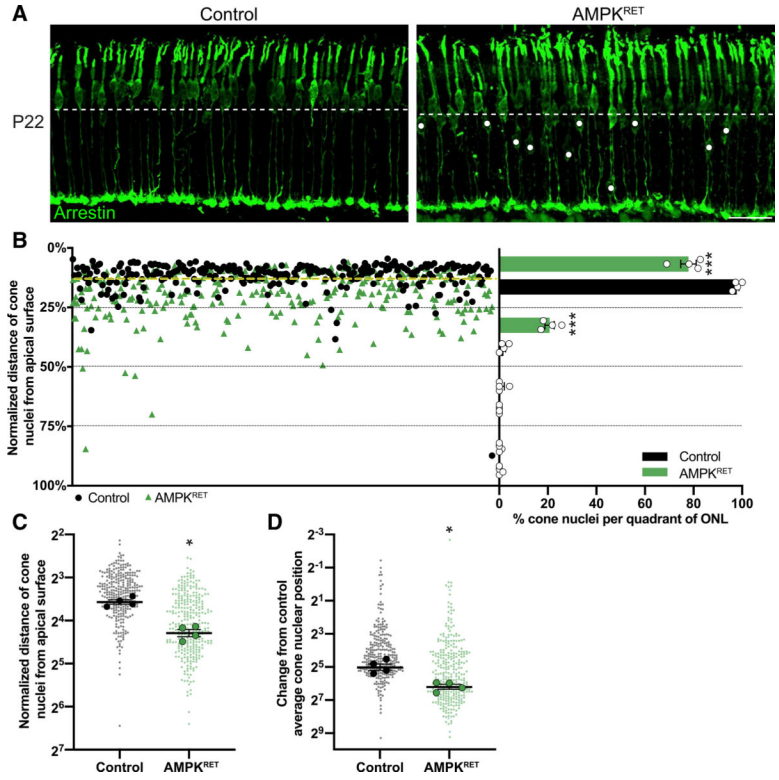

Figure 3. AMPK regulates cone nuclear position

(A) Representative images of cones (anti-arrestin, green) in control and *AMPK*^{RET} mice at P22. Many *AMPK*^{RET} cones display nuclear position defects (white dots). The white dashed line indicates the lower boundary of ONL Q1.

(B) Scatterplot and graph displaying the location and percent quantification of cone nuclei normalized to the length of the ONL in control (black) and *AMPK*^{RET} mice (green) in each ONL quadrant. There is a significant decrease in the number of *AMPK*^{RET} nuclei in the outer half of the ONL relative to controls (n = 292 and 306 cells from 4 control and 4 *AMPK*^{RET} mice, respectively). The yellow dashed line indicates the average normalized cone nuclear position in controls.

(C and D) Quantification of the average normalized distance of cone nuclei from the apical surface of the outer retina (C) and the average nuclear displacement from control cone nuclear position (D). There is a significant increase in both the average distance and the average nuclear displacement of *AMPK*^{RET} mice relative to controls (n = 292 and 306 cells from 4 control and 4 *AMPK*^{RET} mice, respectively).

Scale bars, 25 μm. Data are represented as mean ± SEM (B) or as beeswarm SuperPlots (C and D) in which individual cone nuclei values are presented together with the mean from each animal ± SEM. ***p < 0.001, unpaired two-tailed Student's t test in (B); *p < 0.05, non-parametric Mann-Whitney rank-sum U test (C and D).

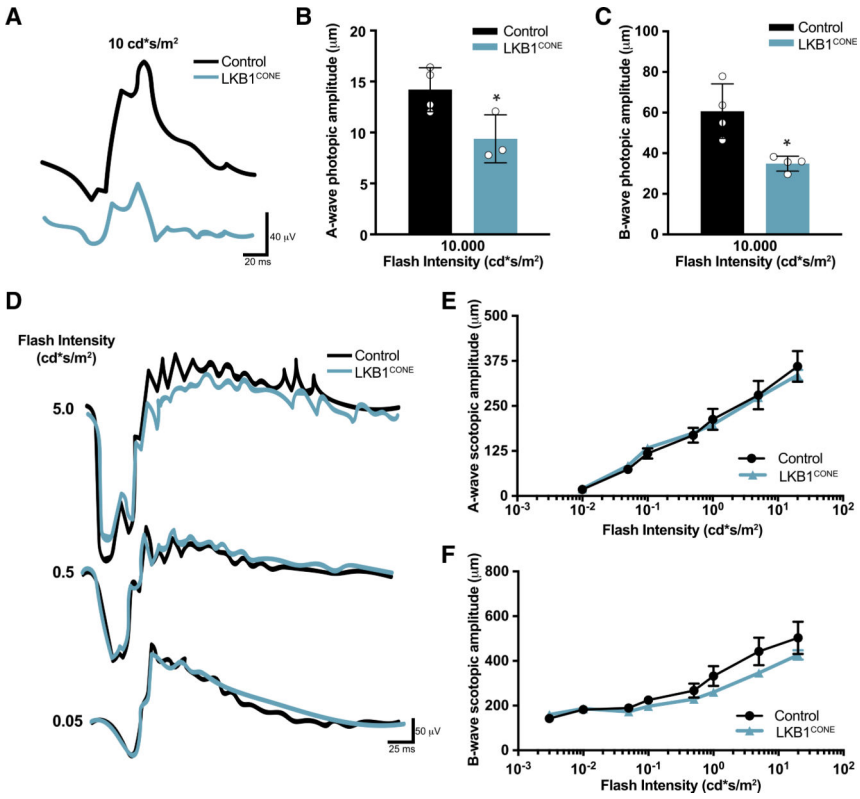

Figure 4. Loss of LKB1 in cones leads to reduction in photopic but not scotopic retinal function

(A) Representative trace of photopic recordings from control and *LKB1*^{CONE} mice.

(B and C) The photopic a-wave (B) and b-wave (C) are significantly reduced in *LKB1*^{CONE} mice.

(D) Representative trace of scotopic recordings from control and *LKB1*^{CONE} mice at different flash intensities.

(E and F) The scotopic a-wave (E) and b-wave (F) are not significantly altered in *LKB1*^{CONE} mice. n = 4 control and 4 *LKB1*^{CONE} mice. Data are represented as mean ± SEM. *p < 0.05, unpaired two-tailed Student's t test.